Advanced Composite Materials
Publication details, including instructions for authors and subscription information:
http://www.tandfonline.com/loi/tacm20

Particle size distribution effects on physical properties of injection molded HA/PLA composites

Tetsuo Takayama [a], Kazuyasu Uchiumi [a], Hiroshi Ito [a], Takahiro Kawai [a] & Mitsugu Todo [b]

[a] Graduate School of Science and Engineering, Yamagata University, Yonezawa, Yamagata, 992-8510, Japan

[b] Research Institute for Applied Mechanics, Kyushu University, Kasuga, Fukuoka, 816-8580, Japan

Published online: 22 Jul 2013.

To cite this article: Tetsuo Takayama, Kazuyasu Uchiumi, Hiroshi Ito, Takahiro Kawai & Mitsugu Todo (2013) Particle size distribution effects on physical properties of injection molded HA/PLA composites, Advanced Composite Materials, 22:5, 327-337, DOI: 10.1080/09243046.2013.820123

To link to this article: http://dx.doi.org/10.1080/09243046.2013.820123

Advanced Composite Materials, 2013
Vol. 22, No. 5, 327–337, http://dx.doi.org/10.1080/09243046.2013.820123

Particle size distribution effects on physical properties of injection molded HA/PLA composites

Tetsuo Takayama[a]*, Kazuyasu Uchiumi[a], Hiroshi Ito[a], Takahiro Kawai[a] and Mitsugu Todo[b]

[a]*Graduate School of Science and Engineering, Yamagata University, Yonezawa, Yamagata 992-8510, Japan;* [b]*Research Institute for Applied Mechanics, Kyushu University, Kasuga, Fukuoka 816-8580, Japan*

(*Received 13 March 2013; accepted 25 June 2013*)

Effects of particle size distribution on physical properties such as viscosity, heat and mechanical properties of injection-molded hydroxyapatite (HA)/poly lactic acid (PLA) were investigated. The melting temperature of PLA was shifted to a lower temperature because of the dispersion of HA particles. However, the cold crystallization temperature shifted to a lower temperature at high HA composition, suggesting that HA particles acted as a nuclear agent. $x_{c,PLA}$ of the composites with bimodal particle size distribution showed the lowest of all three composites, suggesting that mobility of PLA polymer chain was reduced by bimodal particle size distribution, which means the increase of restriction at interface between polymer matrix and particle. Melt flow rate (MFR) increased because of dispersed HA particle. The reason was thought that hydrolysis degradation of PLA occurred during melt-mixing process is accelerated by HAp particle dispersion. The MFR of composites increased concomitantly with increased particle size. Mechanical properties such as flexural strength and the modulus of bimodal-HA/PLA composite with both 5 and 1 μm of representative size were higher than those of monomodal-HA/PLA composites with 5 or 1 μm of representative size within the range of the results of this paper. Fracture surfaces were affected by the particle size distribution. It was suggested for the reasons to relate the interparticle distance and restriction of the interface between the matrix and particles.

Keywords: poly lactic acid; particle size distribution; flexural strength; lubricant effect; crystallinity; bio-absorbable composites

1. Introduction

Poly(lactic acid) (PLA), a bio-absorbable polymer, has biocompatibility. For that reason, it has been used widely for bone-fixation devices used in orthopedics and oral surgery applications.[1–2] Blending with bioactive ceramics such as hydroxyapatite (HA) and β-tricalcium phosphate has recently been undertaken to improve the bioactivity, degradation rate, and stiffness of such medical devices.[3–17] The mechanical properties of dispersed particle composites are well known to depend strongly on the interfacial structure, dispersibility, particle size distribution, and other factors. Many researchers have emphasized the effects of interfacial structure and dispersibility.[18–20] However,

*Corresponding author. Email: t-taka@yz.yamagata-u.ac.jp

the effect of the particle size distribution has not been elucidated to date. Our research group reported the effects of particle size distribution on the mechanical properties of HA/PLA composites. Those results suggest that mechanical properties can be improved by dispersed HA particles with both 5 μm and 100 nm of representative size.[21] However, relations between the particle size and physical properties such as viscosity, thermal, and mechanical properties remain unclear.

In this study, the fabrication process of HA/PLA composites with different particle size distribution was investigated using injection molding. Then the composites' physical properties such as melt flow rate (MFR), density, thermal, and mechanical properties were measured to examine the effects of the particle size distribution on these properties. The HA distribution and fracture surface morphology were also characterized using scanning electron microscopy. The relation between the microstructure and the physical properties was discussed based on experimentally obtained results.

2. Experimental procedure

2.1. Materials and melt-mixing

HA particles (Sangi Co. Ltd.) with representative sizes of about 1 and 5 μm were used as filler. Figure 1 shows the particle size distribution of HA particles. PLA (Lacea® H-100 J; Mitsui Chemicals Inc.) was used as matrix. HA particles and PLA were mixed using a twin screw extruder (IMC-188F, Imoto machinery Co. Ltd.) at 190 °C and 50 rpm. The weight fraction of the HA particles was fixed at 30 wt.%. For composites having both 5 and 1 μm, the weight fraction was 15 wt.% for both particles. The three kinds of HA/PLA composites fabricated are denoted as 5 μ, 1 μ, and 5 μ/1 μ hereinafter. For comparison, neat PLA was also fabricated using the same process.

2.2. Measurements of density and thermal properties

Densities of HA/PLA composites were measured using the sink/float method to estimate HA content with the mixture. The crystallinity values, $x_{c,PLA}$, of PLA in the composites were determined using a modulated differential scanning calorimeter (M-DSC, Q-200; TA Instruments). Samples of the composites were heated under nitrogen gas flow at a

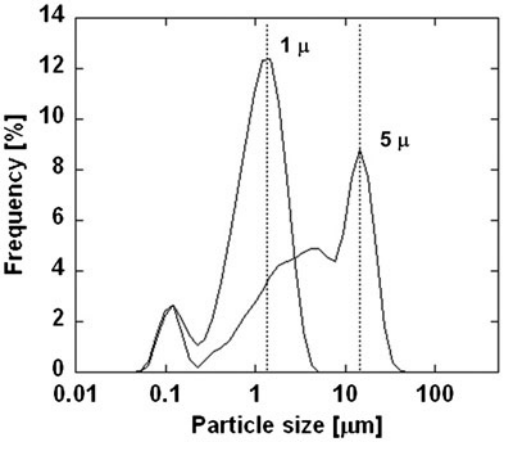

Figure 1. Particle size distribution of HA particles.

rate of 3 °C/min for M-DSC measurements. The enthalpy of crystallization and melting, dH_c and dH_m, were determined using M-DSC. Then $x_{c,PLA}$ was evaluated according to the following formula [22,23]:

$$x_{c,PLA}(\%) = \frac{100 \times (dH_m + dH_c)}{93 \times X_{PLA}} \quad (1)$$

where 93 (J/g of the polymer) is the enthalpy of melting of the PLA crystal having the infinite crystal thickness reported by Fischer et al. [24]. X_{PLA} is the weight fraction of PLA. In addition, the specific heat was measured to evaluate the effective thickness of the interface in M-DSC.

The MFR of mixtures was evaluated using a melt flow indexer. The testing temperature and load were chosen, respectively, as 170 °C and 2.160 kg.

2.3. Injection molding

The fabricated mixtures were pelletized. Then the pellets were dried at 60 °C for at least 12 h in a vacuum constant-temperature oven. Beam specimens with $60 \times 5.5 \times 0.5\,mm^3$ were fabricated using a micro-injection molding machine (Modulated-AU3E; Nissei Plastic Industrial Co. Ltd.). Injection and mold temperature were fixed, respectively, at 180 and 30 °C. Injection speed was also fixed at 100 mm/min.

For comparison, the same specimens were also fabricated by hot-press molding at 180 °C of press temperature.

2.4. Mechanical testing and SEM observation

Three-point bending tests were conducted at a loading-rate of 2 mm/min at a test temperature of 37 °C using a universal mechanical testing machine attached with thermostatic chamber (IMC-18E0, Imoto machinery Co. Ltd.). The span length was denoted as 16 mm. The flexural strength, σ_f, and flexural modulus, E, were evaluated using the following formulas [25]:

$$\sigma_f = \frac{3PL}{2bh^2}, \quad E = \frac{\sigma_1 - \sigma_2}{\varepsilon_1 - \varepsilon_2} \quad (2)$$

where L is the span, b and h respectively denote the width and thickness, and P is the maximum load. σ_1 and σ_2 respectively signify the stresses at $\varepsilon_1 = 0.0025$ and $\varepsilon_2 = 0.0005$. The flexural strength and flexural modulus were averaged over five specimens for each material. The standard deviation was also evaluated.

The HA distribution and fracture surface of the specimens were also observed using a scanning electron microscope (SEM).

3. Results and discussion

3.1. Thermal properties

Figure 2 shows DSC profiles of HA/PLA composites fabricated by press and injection molding. Results show that the melting temperature of PLA was shifted to a lower temperature because of a dispersion of HA particles. The decrease of melting temperature of the injection molding parts was greater than that of press molding parts. Results

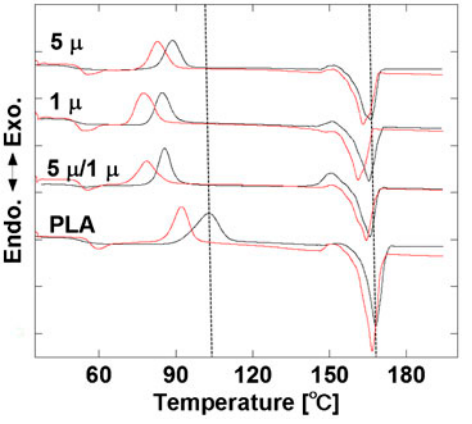

Figure 2. DSC profiles of PLA and HA/PLA composites: black lines present results of press molding; red lines show those of injection molding.

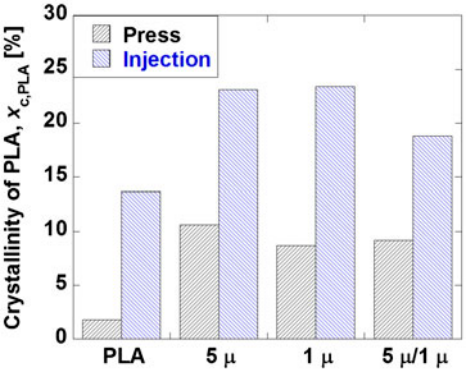

Figure 3. Crystallinity of PLA, $X_{c,PLA}$ of HAp/PLA composites before and after injection molding.

suggest, however, that the cold-crystallization temperature also shifted to a lower temperature at high HA composition. Figure 3 shows the crystallinity of PLA, $x_{c,PLA}$, of HA/PLA composites. It is readily apparent that $x_{c,PLA}$ increased at high HA composition, suggesting that HA particles acted as the nuclear agent for crystallization. In addition, $x_{c,PLA}$ of injection molded composites showed higher values than press molded composites, suggesting that oriented crystallization occurred during injection molding. $x_{c,PLA}$ of the composites with bimodal particle size distribution showed the lowest of all three composites, suggesting that mobility of PLA polymer chain was reduced by bimodal particle size distribution, which means the increase of restriction at interface between polymer matrix and particle. Such increase is thought to improve the interfacial strength.

3.2. MFR and density

Figure 4 shows MFR of HA/PLA composites fabricated using a press and injection molding. Results show that the MFRs of all composites were higher than those of neat

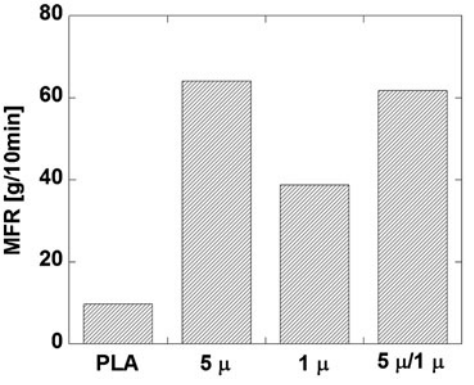

Figure 4. MFRs of HA/PLA composites.

Table 1. Densities of HA/PLA composites.

Code	Density (g/cm^3)	Calculated density (g/cm^3)	Increment (g/cm^3)	HA content (vol.%)	HA content (wt.%)
PLA	1.241	1.241	0.000	0.00	0.00
5 μ	1.498	1.564	0.066	13.3	28.2
1 μ	1.499	1.564	0.065	13.4	28.3
5 μ/1 μ	1.496	1.564	0.068	13.2	28.0

PLA. In general, incorporation of particles increase viscosity which result in lower MFR, however this result shows the opposite tendency. It is thought to be that hydrolysis degradation of PLA occurred during melt-mixing process is accelerated by HAp particle dispersion, because HAp has the hydroxyl group as functional group. Effect of hydrolysis degradation on the decrease of viscosity is larger than effect of incorporation of particles on the increase of viscosity, resulting that viscosity decrease which results in higher MFR. In addition, the MFR increased concomitantly with increased particle size. Table 1 presents the densities of HA/PLA composites obtained using a sink/float method. The density increased by HA particle dispersion, but the densities of composites were unaffected by the particle size distribution, suggesting that HA contents of the composites were almost constant.

3.3. Particle distribution observation

Figure 5 shows the HA particle distribution in the injection molded parts. These figures were observed by slicing with a microtome to obtain a cross section of thin specimen. For 5 μ and 5 μ/1 μ shown in Figure 5(a) and (b), HA particles of about 5–10 μm were visible. These particles were dispersed homogeneously. Figure 5(c) shows that such particles were invisible at this magnification, suggesting that the 1 μm HA particles were dispersed homogeneously.

3.4. Mechanical properties

Figure 6 portrays typical stress–strain curves of HA/PLA composites obtained from three-point bending tests. The maximum stress of 5 μ/1 μ was the highest of all three

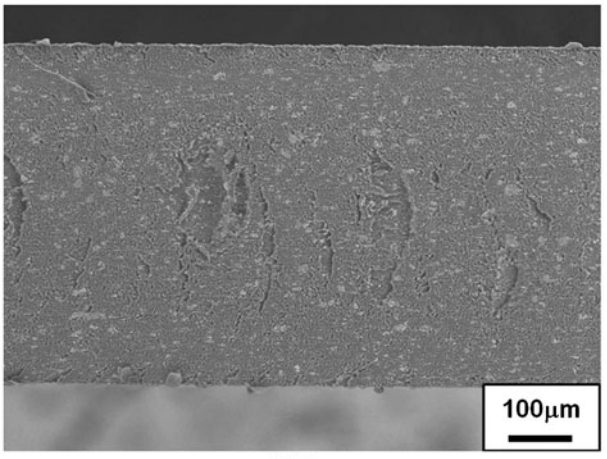

(a) 5 μ

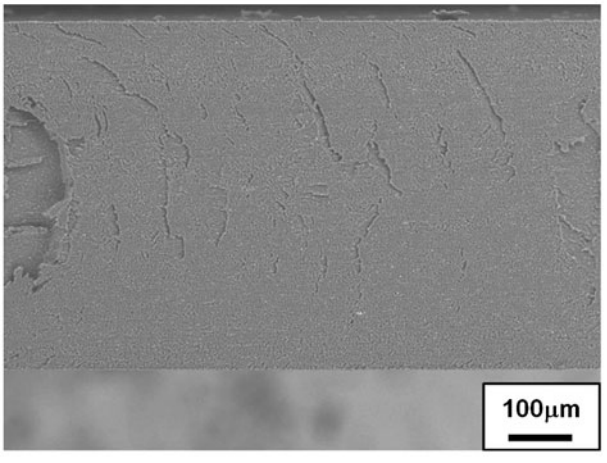

(b) 1 μ

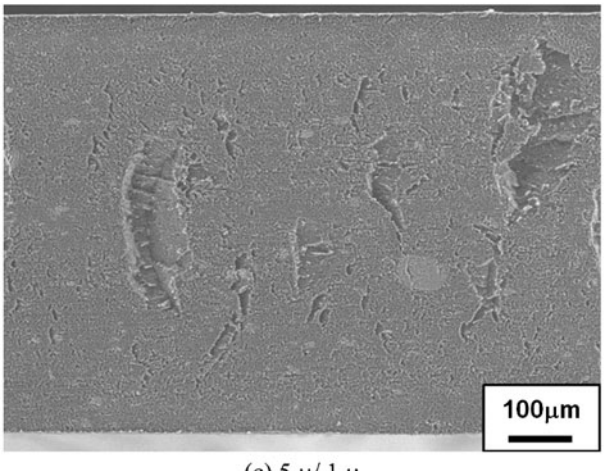

(c) 5 μ/ 1 μ

Figure 5. SEM micrographs of HA particles distribution of injection molding parts.

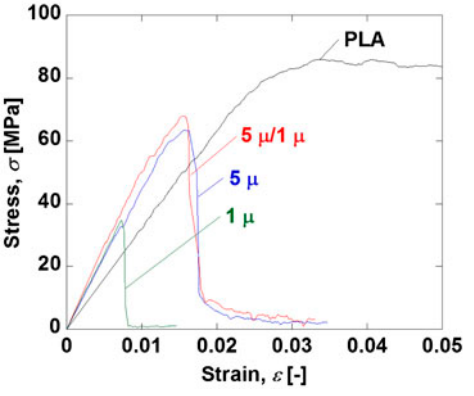

Figure 6. Stress–strain curves of PLA and HA/PLA composites obtained from three-point bending tests conducted at 37 °C.

composites. The maximum stress of 5 μ was comparable to that of 5 μ/1 μ, but 1 μ exhibited the lowest peak stress, indicating a dramatic decrease of flexural strength. It was noted that the sudden drop of load after the peak corresponded to brittle fracture behavior in all the composites. The flexural properties are presented in Figure 7. Of all

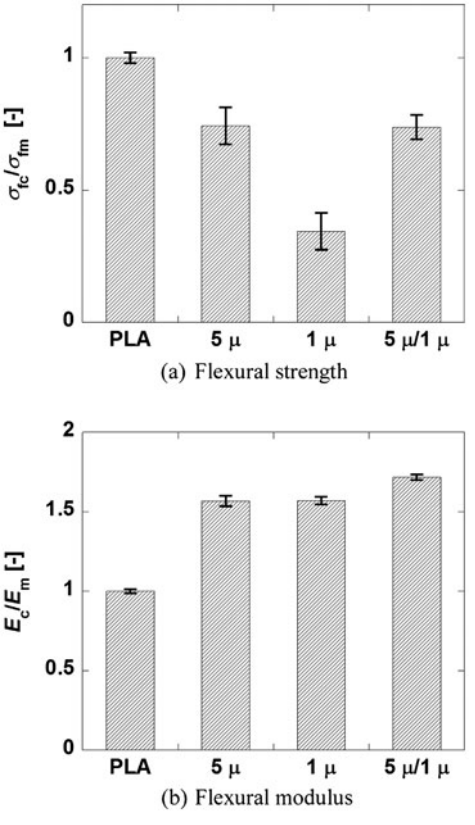

Figure 7. Flexural properties of HA/PLA composites at 37 °C.

three composites, 5 μ/1 μ exhibited the highest σ_f value, but this value was lower than that of PLA. The 1 μ composite exhibited the lowest strength: it was much lower than that of either 5 μ/1 μ or 5 μ. The 5 μ/1 μ composite showed the highest E value. From all results, bimodal-HA/PLA exhibited the best performance of any composite.

3.5. *Fracture surface observation*

Figure 8 shows the fracture surfaces of thin specimens in the tensile regions. The fracture surface of 1 μ showed a very smooth and flat surface, as depicted in Figure 8(a). The interparticle distance is known to depend on the particle diameter and volume fraction of particles. In this case, because the volume fraction of HA particles was almost identical, the interparticle distance of HA/PLA composites depends on the particle diameter. The interparticle distance of smaller particles such as 1 μ is shorter than that of larger particles

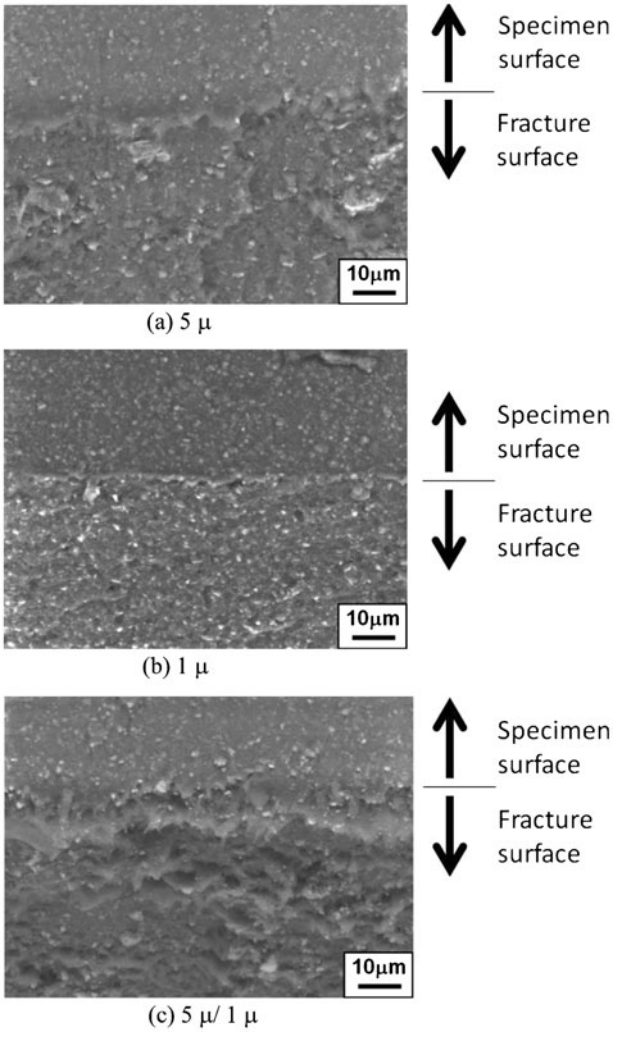

Figure 8. SEM micrographs of fracture surface at the tensile region obtained from three-point bending tests.

such as 5 μ. Consequently, it is considered that the PLA matrix deformation near the particles is reduced because of the restriction of the interface between the matrix and particles and that unstable deformation occurs easily under the lower stress condition, resulting in the lowest σ_f presented in Figure 7.

It is also apparent from Figure 8(b) that 5 μ exhibited a rougher surface than 1 μ did. Such a rough surface was characterized by interfacial failure at the interfaces between HA particles and PLA matrix. It is also noteworthy that localized ductile deformation of matrix existed in the surroundings of the debonded particles. For 5 μ, the interparticle distance becomes larger than that of 1 μ, considering that such unstable deformation reduced under the lower stress condition and localized ductile deformation corresponding to the stable deformation occurs slightly, resulting in the middle σ_f, as presented in Figure 7. In 5 μ/1 μ, localized ductile deformation of matrix was visible more than in 5 μ. It is noteworthy that the interparticle distance of 5 μ/1 μ is intermediate of all the composites because particles of both 5 and 1 μ are dispersed, considering that the unstable deformation such as 1 μ is reduced. Therefore, the localized ductile deformation such as 5 μ is also reduced, considering that the void formation attributable to the debonded particles is reduced by improvement of interfacial strength. Consequently, such reductions engender the ductile deformation of matrix under higher stress conditions, resulting in the highest σ_f, as presented in Figure 7.

4. Summary

In this study, effects of HA distribution on the physical properties such as MFR, density, thermal and mechanical properties were investigated. Results were obtained as follows:

(1) The melting temperature of PLA was shifted to a lower temperature because of the HA particle dispersion. However, the cold crystallization temperature shifted to a lower temperature at high HA composition, suggesting that HA particles acted as a nuclear agent. $x_{c,PLA}$ of the composites with bimodal particle size distribution showed the lowest of all three composites, suggesting that mobility of PLA polymer chain was reduced by bimodal particle size distribution, which means the increase of restriction at interface between polymer matrix and particle.
(2) MFR increased because of HA particle dispersion. The reason was thought that hydrolysis degradation of PLA occurred during melt-mixing process is accelerated by HAp particle dispersion. The MFR of composites increased concomitantly with increased particle size.
(3) Density tended to increase by HA particle dispersion, but it was unaffected by the particle size distribution, suggesting that the HA contents of composites fabricated in this study are almost constant.
(4) Mechanical properties such as flexural strength and the modulus of bimodal-HA/PLA composite with both 5 and 1 μm representative sizes were higher than those of monomodal-HA/PLA composites with 5 or 1 μm of representative size within the range of the results of this paper.
(5) Fracture surfaces were affected by the particle size distribution. It was suggested for the reasons to relate the interparticle distance and restriction of the interface between the matrix and particles.

References

[1] Leenslag JW, Pennings AJ, Bos RRM, Rozema FR, Boering J. Resorbable materials of poly (L-lactide). IV. Plates and screws for internal fracture fixation. Biomaterials. 1987;8:70–73.

[2] Bostman OM. Absorbable implants for the fixation of fractures. J. Bone Joint Surg. 1991;73-A:148–153.

[3] Shikinami Y, Okuno M. Bioresorbable devices made of forged composites of hydroxyapatite (HA) particles and poly L-lactide (PLLA): part I. Basic characteristics. Biomaterials. 1999;20:859–877.

[4] Yasunaga T, Matsusue Y, Furukawa T, Shikinami Y, Okuno M, Nakamura T. Bonding behavior of ultrahigh strength unsintered hydroxyapatite particles/poly(L-lactide) composites to surface of tibial cortex in rabbits. J. Biomed. Mater. Res. 1999;47:412–419.

[5] Kasuga T, Ota Y, Nogami M, Abe Y. Preparation and mechanical properties of polylacyic acid containing hydroxyapatite fibers. Biomaterials. 2001;22:19–23.

[6] Rizzi SC, Heath DJ, Coombes AGA, Bock N, Textor M, Downes S. Biodegradable polymer/hydroxyapatite composites: Surface analysis and initial attachment of human osteoblasts. J. Biomed. Mater. Res. 1999;47:475–486.

[7] Furukawa T, Matsusue Y, Yasunaga T, Nakagawa Y, Okada Y, Shikinami Y, Okuno M, Nakamura T. Histomorphometric study of high-strength hydroxyapatite/poly(L-lactide) composite rods for internal fixation of bone fractures. J. Biomed. Mater. Res. 2000;50:410–419.

[8] Furukawa T, Matsusue Y, Yasunaga T, Shikinami Y, Okuno M, Nakamura T. Biodegradation behavior of ultra-high-strength hydroxyapatite/poly(L-lactide) composite rods for internal fixation of bone fractures. Biomaterials. 2000;21:889–898.

[9] Deng X, Hao J, Wang C. Preparation and mechanical properties of nanocomposites of poly (D,L-lactide) with Ca-deficient hydroxyapatite nanocrystals. Biomaterials. 2001;22:2867–2873.

[10] Shikinami Y, Matsusue Y, Nakamura T. The complete process of bioresorption and bone replacement using devices made of forged composites of raw hydroxyapatite particles/poly L-lactide (F-u-HA/PLLA). Biomaterials. 2005;26:5542–5551.

[11] Hong Z, Zhang P, He C, Qiu X, Liu A, Chen L, Chen X, Jing X. Nano-composite of poly (L-lactide) and surface grafted hydroxyapatite: mechanical properties and biocompatibility. Biomaterials. 2005;26:6296–6304.

[12] Debra DWC, Julia AK, Darinda MM, Cho LM. In vitro flexural properties of hydroxyapatite and self-reinforced poly(L-lactic acid). J. Biomed. Mater. Res. Part A. 2006;78-A:541–549.

[13] Fang L, Yan J, Xiaodan L, Demin J. Properties and morphology of bioceramics/poly(D, L-lactide) composites modified by *in situ* compatibilizing extrusion. J. Appl. Polym. Sci. 2006;102:4085–4091.

[14] Kikuchi M, Suetsugu Y, Tanaka J. Preparation and mechanical properties of calcium phosphate/copoly-L-lactide composites. J. Mater. Sci. – Mater. Med. 1997;8:361–364.

[15] Verheyen CCPM, de Wijn JR, van Blitterswijk CA, de Groot K. Evaluation of hydroxyapatite/poly(L-lactide) composites: mechanical behavior. J. Biomed. Mater. Res. 1992;26:1277–1296.

[16] Yamaji S, Kobayashi S. Effect of *in vitro* hydrolysis on the compressive behavior and strain rates dependence of tricalcium phosphate/poly(L-lactic acid) composites. Adv. Compos. Mater. 2013;22:1–11.

[17] Kobayashi S, Sakamoto K. Bending and compressive properties of crystallized TCP/PLLA composites. Adv. Compos. Mater. 2009;18:287–295.

[18] Liu T, Phang IY, Shen L, Chow SY, Zhang WD. Morphology and mechanical properties of multiwalled carbon nanotubes reinforced nylon-6 composites. Macromolecules. 2004;37:7214–7222.

[19] Park JH, Jana SC. The relationship between nano- and micro-structures and mechanical properties in PMMA-epoxy-nanoclay composites. Polymer. 2003;44:2091–2200.

[20] Qu Y, Yang F, Yu ZZ. A new conception on the toughness of nylon-6/silica nanocomposite prepared via *in situ* polymerization. J. Polym. Sci. Part B: Polym. Phys. 1998;36:789–795.

[21] Takayama T, Todo M, Takano A. Effect of bimodal distribution on mechanical properties of hydroxyapatite particles filled poly(L-lactide) composites. J. Mech. Behav. Biomed. Mater. 2009;2:105–112.

[22] Tsuji H, Ikada Y. Properties and morphologies of poly (L-lactide): 1. Annealing condition effects on properties and morphologies of poly (L-lactide). Polymer. 1995;36:2709–2716.

[23] Todo M, Park SD, Takayama T, Arakawa K. Fracture micromechanisms of bioabsorbable PLLA/PCL polymer blends. Eng. Frac. Mech. 2007;74:1872–1883.
[24] Fischer EW, Sterzel HJ, Wegner G. Investigation of the structure of solution grown crystals of lactide copolymers by means of chemical reactions. Kolloid-Z. u. Z Polym. 1973;251:980–990.
[25] Japanese Standards Association. JIS K7171 Plastics – determination of flexural properties. Japanese Industrial Standard Handbook; 2010. p. 492–502.